JAAS
Journal of Analytical Atomic Spectrometry

Accepted Manuscript

This article can be cited before page numbers have been issued, to do this please use: S. Mcheik, E. Da Silva and A. Pejovic-Milic, *J. Anal. At. Spectrom.*, 2026, DOI: 10.1039/D6JA00139D.

ROYAL SOCIETY OF CHEMISTRY

rsc.li/jaas

View Article Online
DOI: 10.1039/D6JA00139D

Journal Name

ARTICLE TYPE

Cite this: DOI: 00.0000/xxxxxxxxxx

The impact of soft-tissue phantoms on the *in vivo* quantification of lead in bone using portable X-ray fluorescence spectrometry

Sajed Mcheik[a]*, Eric Da Silva[a] and Ana Pejović-Milić[a]

Received Date
Accepted Date

DOI: 00.0000/xxxxxxxxxx

Portable X-ray fluorescence spectrometry (pXRF) has emerged as a promising technique for the *in vivo* quantification and monitoring of bone lead (Pb) through the detection of characteristic Pb L X-rays. Accurate calibration requires bone and soft-tissue surrogates that replicate photon attenuation and scattering at the measurement site. While significant efforts have focused on bone-mimicking materials, less attention has been given to soft-tissue equivalents.

In this study, two soft-tissue mimicking materials—Lucite (PMMA) and paper (98% cellulose)—with thicknesses ranging from 0 to 7 mm were investigated and compared with porcine tissue, which closely approximates human soft tissue. The experimentally determined experimentalmass attenuation coefficients for Pb L X-rays at 10.5 keV were 5.22, 4.17, and 4.94 cm^2/g for Lucite, paper, and porcine tissue, respectively, indicating that paper provides attenuation properties comparable to those of soft tissue.

Calibration curves were generated using six hydroxyapatite (HAp) bone phantoms doped with Pb at varying concentrations and measured for 180 s live time using a Niton XL5 spectrometer (Thermo Fisher Scientific, USA) operating at 40 kVp using an aluminum (Al) filter. At 2.00 mm thickness, the minimum detection limits (MDLs) were 2.2, 1.7, and 2.2 μg Pb/g Ca for Lucite, paper, and porcine tissue, respectively. At 5.00 mm, the MDLs increased to 10.6, 4.3, and 6.2 μg Pb/g Ca.

Pb concentrations in three cadaveric tibiae overlaid with porcine tissue were quantified using direct calibration, adjusted coherent normalization, and Compton interpolation. No significant differences were observed among the methods ($p > 0.05$) using Lucite. Despite paper showing attenuation coefficients closer to porcine tissue, Lucite more accurately reproduced the combined attenuation and scattering behaviour of human soft tissue, supporting its use *in vivo* pXRF calibration.

1 Introduction

A pXRF spectrometer utilizes an X-ray tube to excite elements of interest within the bone matrix, which subsequently emit characteristic X-rays upon relaxation. pXRF has been proposed as an *in vivo* diagnostic tool due to its non-destructive and non-invasive nature, relatively low radiation dose, portability, and cost-effectiveness compared to conventional laboratory-based techniques such as atomic absorption spectroscopy (AAS) and inductively coupled plasma (ICP) methods. To date, portable X-ray fluorescence (pXRF) has been used to quantify several elements in human bone, including Pb[1–3], Sr[2,4], Cd and As[5], as well as P, K, Ca, Fe, and Zn[6].

Lead (Pb) is one of the most extensively studied elements in human bone due to its toxicity, widespread environmental exposure, and significant adverse health effects[7]. Human exposure to Pb and its associated health risks have been well documented in the literature and by the U.S. Centers for Disease Control and Prevention[8]. Exposure to Pb has been linked to cardiovascular, neurological, and renal damage[8]. Furthermore, even low-level exposure (< 10 μg/dL in blood) has been associated with intellectual impairment in children[9] and increased mortality risk[10,11]. According to biokinetic models, approximately 94% of systemic Pb is stored in the skeleton[12], with half-lives in cortical bone (e.g., tibia) ranging from 7 to 26 years[13]. This prolonged retention supports the use of *in vivo* bone Pb X-ray fluorescence (XRF) as a reliable method for assessing long-term exposure[1,13,14].

Accurate calibration of pXRF systems requires that both bone and soft-tissue phantom materials replicate the attenuation and scattering properties of human tissues. For Pb L-line XRF systems, calibration is typically performed using bare bone phantoms, while the effects of overlying soft tissue are accounted for by measuring or estimating tissue thickness and applying attenuation corrections to the detected Pb signal. Bone phantoms used

[a] Department of Physics, Faculty of Science, Toronto Metropolitan University, 350 Victoria Street, Toronto, ON M5B 2K3; E-mail: smcheik@torontomu.ca

View Article Online
DOI: 10.1039/D6JA00139D

for calibration include plaster of Paris[15], bone meal[16], and hydroxyapatite (HAp)[17,18].

Lucite (PMMA) is widely used as a soft-tissue phantom material in XRF applications[3,4,15,16]. Its composition—primarily carbon, hydrogen, and oxygen—with an effective atomic number ($Z_{\text{eff}} \approx 6.6$) closely approximates that of human soft tissue (ICRU-44) ($Z_{\text{eff}} \approx 7.4$)[19], resulting in similar X-ray interaction characteristics. Additionally, Lucite is inexpensive, readily available, and easy to machine. However, Lucite has primarily been used to estimate soft-tissue thickness rather than to generate calibration curves across a range of tissue thicknesses. Nie *et al.*[3] proposed estimating human soft-tissue thickness using the dependence of the Compton peak on Lucite thickness, assuming similar scattering behaviour between Lucite and biological tissue. This approach provides an alternative to ultrasound or other imaging modalities for determining overlying tissue thickness[20].

Besides Lucite, paper (98% cellulose) has recently been proposed as a soft-tissue surrogate for bone strontium measurements based on K-shell X-ray emissions ($K_\alpha = 14.1$ keV), which lie within a similar energy range to the Pb L X-rays ($L_\alpha = 10.5$ keV and $L_\beta = 12.6$ keV) used in pXRF measurements. Cellulose, composed primarily of carbon, hydrogen, and oxygen, has an effective atomic number ($Z_{\text{eff}} \approx 6.9$), which is comparable to that of Lucite but lower than that of ICRU-44 soft tissue. However, similarity in effective atomic number alone does not fully describe photon attenuation and scattering behaviour in heterogeneous materials.

For measurements based on low-energy X-ray emissions, attenuation by overlying soft tissue must be carefully accounted for. Ultrasound imaging is commonly used to determine soft-tissue thickness at the measurement site[20,21]. Magnetic resonance (MR) and computed tomography (CT) imaging have also been explored; however, these techniques are less accessible, more costly, and, in the case of CT, contribute additional radiation dose[20].

The minimum detection limit (MDL) is a key metric used to evaluate the performance of XRF measurements and their sensitivity for detecting elements of interest. In *in vivo* XRF systems, the MDL is typically calculated as[22]:

$$\text{MDL} = \frac{2\sigma}{m} \tag{1}$$

where σ represents the standard deviation of the signal measured from the 0 μg Pb/g Ca phantom, and m is the slope of the calibration curve (i.e., the sensitivity). When both Pb L_α (10.5 keV) and L_β (12.6 keV) peaks are used, the combined MDL is calculated using a reduced mean square formulation[23]:

$$\text{MDL} = \sqrt{\frac{1}{\frac{1}{\text{MDL}_{L_\alpha}^2} + \frac{1}{\text{MDL}_{L_\beta}^2}}} \tag{2}$$

Although *in vivo* bone Pb L-XRF has been applied in recent years to monitor Pb concentrations in humans[1,3,13], limited attention has been given to incorporating soft-tissue materials directly into calibration phantoms. This is largely because existing approaches rely on measuring or estimating overlying soft-tissue thickness and applying attenuation corrections to recover the equivalent bare-bone signal. In this work, soft-tissue materials, specifically Lucite and paper, are investigated as human tissue surrogates for bone Pb pXRF measurements. Additionally, their impact on Pb quantification is evaluated using cadaveric tibiae overlaid with porcine tissue.

2 Experimental

2.1 Preparation of bone-mineral mimicking phantoms

Hydroxyapatite (HAp) [$Ca_{10}(PO_4)_6(OH)_2$] phantoms were prepared to mimic bone mineral, following the method described by Da Silva et al.[17,24,25]. The phantoms were synthesized using mixtures of $CaHPO_4 \cdot 2H_2O$ (30.83 g) and $Ca(OH)_2$ (8.85 g), combined to achieve a Ca/P molar ratio of 1.67. The phantoms were doped with Pb using a certified standard solution of 1031 μg/g (VWR International, Radnor, PA, USA; nominal concentration 1000 μg/g), to prepare six bone phantoms with Pb concentrations of 0, 5, 10, 20, 50, and 100 μg Pb/g Ca. The total mass of the dried powder mixture for each phantom was 50 g prior to the addition of a 1 M sodium phosphate dibasic setting solution (Na_2HPO_4, ACS reagent, $\leq$99.0%, Sigma-Aldrich, Japan). The mixtures were thoroughly homogenized and transferred into plastic weighing boats, resulting in phantoms with a thickness of approximately 1.5 cm and a diameter of 6.0 cm after air drying.

2.2 Overlaying soft-tissue phantoms and experimental mass attenuation

At the tibia bone Pb measurement site, commonly used in bone Pb XRF studies, the average thickness of the overlying soft tissue ranges between (3.6 ± 1.5) mm[26] and (4.8 ± 2.0) mm[27]. In the case of phalanx bone measurements also used in bone Sr and Pb XRF applications, the average soft-tissue thickness is (2.9 ± 0.7) mm[27]. Therefore, the range of soft-tissue thicknesses investigated in this work was selected to represent those encountered in tibia and phalanx *in vivo* measurements. Two soft-tissue surrogate materials were investigated: Lucite (Langaelex, China) and paper (98% cellulose, Whatman grade 4 filter paper, China). Lucite sheets were laser-cut into 3×3 cm pieces with a thickness of (1.15 ± 0.05) mm. Multiple layers were stacked to obtain total thicknesses of 1.15, 2.30, 3.45, 4.60, 5.75, and 6.90 mm. The paper-based soft-tissue phantom was prepared using Whatman grade 4 filter paper (98% cellulose), with individual sheet thickness of 1.00 mm. Sheets were stacked to achieve total thicknesses of 1.00, 2.00, 3.00, 4.00, 5.00, 6.00, and 7.00 mm. Porcine tissue, assumed to approximate human soft tissue, was used to cover cadaveric tibiae to simulate *in vivo* measurement conditions. Tissue samples were obtained from porcine belly and prepared with thicknesses of 1.25, 3.00, 4.00, 5.00, and 6.50 mm. The thickness of all soft-tissue samples was measured using a Vernier caliper with an uncertainty of (± 0.05) mm.

The linear attenuation coefficient of each soft-tissue mimicking material was determined by fitting the variation of the Pb signal (100 μg Pb/g Ca HAp phantom) as a function of soft-tissue thickness using the Beer–Lambert law. The experimentalmass attenuation coefficient was then obtained by dividing the linear attenuation coefficient by the density of the corresponding material.

View Article Online
DOI: 10.1039/D6JA00139D

2.3 Cadaver Tibia Bones

Three untreated postmortem tibiae were acquired from Mount Sinai Allograft Technologies (Toronto, Ontario, Canada), with donor consent obtained through the Trillium Gift of Life Network, the provincial organ and tissue donation authority. Mount Sinai Allograft Technologies, accredited by Health Canada and the American Association of Tissue Banks, provides bone and tissue exclusively to institutions operating under approved research ethics board protocols. The tibiae were stored at $-70\,^{\circ}\mathrm{C}$ and screened for infectious agents, including hepatitis and HIV. All experiments were performed in accordance with the guidelines of Health Canada, and experiments were approved by the ethics committee at Toronto Metropolitan University. Residual soft tissue was removed from the bone shafts using a stainless-steel knife to produce a clean irradiation surface comparable to that of bare hydroxyapatite (HAp) phantoms. During pXRF measurements, the flattest surface of each triangular tibial cross-section was oriented toward the detector.

2.4 Lead Quantification in Cadaver Tibiae

The three cadaveric tibiae were measured with soft-tissue materials overlaid at the mid-point of each bone. The same soft-tissue thicknesses were used for both HAp phantoms and cadaveric tibiae measurements, as described in Section 2.2. Tibiae overlaid with porcine tissue were assumed to simulate the *in vivo* human bone Pb measurement site, while HAp phantoms overlaid with Lucite or paper were used to construct calibration curves for Pb quantification.

Bone Pb quantification in the postmortem tibiae was performed using three approaches: (1) direct quantification, (2) adjusted coherent normalization [28], and (3) Compton interpolation [7,15,29].

Direct quantification is based on calibration curves obtained from HAp phantoms with varying Pb concentrations, each covered with a fixed thickness of soft-tissue material. This approach requires generating multiple calibration curves for both Lucite and paper across different thicknesses. During *in vivo* measurements, knowledge of the overlying tissue thickness is required to select the appropriate calibration curve. In this study, cadaveric tibiae were covered with known porcine tissue thicknesses, eliminating the need for thickness estimation.

Adjusted coherent normalization was adapted from Gevaert and Chettle [28]. While Gevaert and Chettle applied this method for bone Sr quantification using paper as a soft-tissue surrogate, the present work extends the approach to bone Pb quantification. The procedure used to estimate Pb concentration in cadaveric tibiae overlaid with porcine tissue is summarized as follows:

1. Plot the Compton peak area as a function of the thickness of paper and Lucite overlying HAp phantoms to determine the equivalent porcine tissue thickness.
2. Calculate the net peak areas of Pb Lα, Pb Lβ, and coherent (Rayleigh) peaks from tibia measurements.
3. Generate attenuation curves by measuring HAp phantoms with varying thicknesses of Lucite and paper, plotting Pb Lα, Pb Lβ, and coherent peak areas as functions of thickness.
4. Use the equivalent porcine thickness (Step i) and attenuation relationships (Step iii) to estimate unattenuated Pb Lα, Pb Lβ, and coherent peak areas.
5. Construct calibration curves using bare HAp phantoms (no overlying soft tissue materials) by plotting Pb Lα and Pb Lβ peak areas normalized to the coherent peak area as functions of Pb concentration.
6. Determine Pb concentration by applying the ratios of unattenuated Pb peaks to the coherent peak (Step iv) to the calibration curves (Step v).

Compton interpolation [7,15,29] assumes that the Compton peak ($\sim$20.8 keV) is independent of Pb concentration. The method is summarized as follows:

1. Plot Pb Lα and Pb Lβ peak areas as functions of soft-tissue thickness using a 100 μg Pb/g Ca HAp phantom for both Lucite and paper.
2. Estimate the equivalent porcine tissue thickness using the Compton peak area, as described in Step 1 of the adjusted coherent normalization method.
3. Determine Pb concentration using the Compton interpolation equation:

$$[\mathrm{Pb}] = 100\ \mu\mathrm{g\ Pb/g\ Ca} \left(\frac{\text{Pb peak area (tibia, thickness } x)}{\text{Pb peak area (100 } \mu\text{g Pb/g Ca phantom, thickness } x)} \right) \tag{3}$$

2.5 Portable X-ray fluorescence spectrometery

All measurements were performed using a Niton XL5 portable X-ray fluorescence (pXRF) spectrometer (Thermo Fisher Scientific Inc., Boston, MA, USA). The instrument is equipped with an Ag anode X-ray tube and a silicon drift detector (SDD) with an energy resolution of 150–185 eV at Mn Kα (5.9 keV). The system was operated at 40 kVp with a beam spot diameter of approximately 8 mm. The distance between the pXRF window and the sample surface was kept constant by maintaining direct contact between the instrument and the sample, ensuring a fixed measurement geometry and minimizing air attenuation effects. Measurements were conducted in mining mode using the main filter (Al filter at 40 kVp) as recommended by the manufacture for Pb measurements. In this mode, the XL5 is capable of simultaneously detecting multiple elements, including U, Th, Bi, Pb, Au, Hg, Re, W, Ta, Hf, Sb, Sn, Cd, Pd, Ag, Mo, Nb, Zr, Y, Sr, Rb, As, Se, Zn, Cu, Ni, Co, Fe, Mn, Cr, V, and Ti.

2.6 Data and Statistical Analysis

Each sample was measured for 180 s of live time, in triplicate. The collected spectrum was exported and analyzed using MATLAB. The Pb L_α(10.5 keV) and Pb L_β (12.6 keV) peaks, as well as

View Article Online
DOI: 10.1039/D6JA00139D

the background, were fitted using the Levenberg-Marquardt algorithm[30,31]. The fitting of the Pb peak area utilized a custom equation made of a Gaussian function that fits the Pb peak, and a linear function that fits the background below the Pb peak. The peak with the highest concentration was used to determine the peak width, which was fixed for the rest of the peak fitting to minimize the number of variables.

Statistical comparisons between the bare bone Pb measurements and the extrapolated Pb concentrations obtained using the three quantification methods were performed using Welch's *t*-test. Each measurement was based on three independent replicates ($n = 3$). Statistical analyses were performed at the 95% confidence level, and results were considered statistically significant when $p < 0.05$.

3 Results and Discussion

3.1 Bone Pb signal attenuation in soft-tissue materials

The attenuation coefficients derived from Pb L-shell intensities should be interpreted as experimentally determined mass attenuation coefficients rather than true material-specific mass attenuation coefficients. The measured Pb intensity reflects not only attenuation by the overlying soft-tissue substitute, but also attenuation and scattering within the underlying bone or HAp matrix. However, the statistically comparable values obtained for porcine tissue and ICRU soft tissue (Table 1) suggest that the attenuation contribution from the bone matrix is relatively small. This is consistent with the shallow depth from which the Pb L-shell signal originates. Furthermore, because the bone/HAp layer remained constant within each experimental comparison, its contribution was assumed to be consistent across measurements within the experimental uncertainty.

A suitable soft-tissue surrogate should exhibit attenuation and scattering properties comparable to those of human soft tissue. To evaluate the attenuation behaviour of Lucite and paper, their experimental mass attenuation coefficients were experimentally determined and compared with those of porcine tissue and ICRU-44 reference human soft tissue[32].

Table 1 summarizes the experimentally determined experimental mass attenuation coefficients for Lucite, paper, and porcine tissue at the energies corresponding to the Pb L_α (10.5 keV) and Pb L_β (12.6 keV) characteristic peaks. These values were obtained by dividing the linear attenuation coefficients—derived from the variation of Pb L peak areas as a function of material thickness (Figure 1)—by the corresponding material densities (Table 2). The densities of all materials were calculated from their measured mass and volume.

When compared with the ICRU-44 reference human soft-tissue density of 1.06 g/cm^3 [32], the experimentally determined densities showed noticeable differences. This discrepancy is expected, as porcine tissue consists of a heterogeneous mixture of fat and muscle, whereas ICRU-44 soft tissue represents an idealized reference composition. These compositional differences likely account for the observed ~12% deviation between the theoretical human soft-tissue density and the measured density of porcine tissue.

Table 1 Comparison of experimental mass attenuation coefficients for Lucite, paper and porcine with the ICRU-44 human soft-tissue coefficient for Pb L_α and L_β. The theoretical mass attenuation coefficients were calculated using the NIST XCOM database[33]. The percent difference compares experimental values to ICRU-44 soft-tissue coefficients. (*) Statistically significant at $p < 0.05$

Material	Peak	Experimental (cm^2/g)	Theoretical (cm^2/g)	% Diff.	*p*-value
Paper	L_α	4.17 ± 0.20	4.22	9%	0.06
	L_β	2.54 ± 0.30	2.48	8%	0.30
Lucite	L_α	5.22 ± 0.20	5.90	18%	0.02*
	L_β	3.41 ± 0.30	3.46	25%	0.05*
Porcine	L_α	4.94 ± 0.20	–	7%	0.10
	L_β	2.53 ± 0.50	–	9%	0.47
Soft tissue (ICRU-44)	L_α	4.62	–	–	–
	L_β	2.78	–	–	–

Table 2 Calculated densities ($\pm 0.05 g/cm$) of materials used in the study

Material	ρ (g/cm^3)
Paper	0.82
Lucite	1.18
Porcine	1.19

The experimental mass attenuation coefficients of paper and porcine tissue differ by less than 10% at these energies compared to the National Institute of Standards and Technology (NIST) ICRU-44 mass attenuation of human soft-tissue, also included in Table 1. In contrast, Lucite has a significantly higher experimentally determined mass attenuation coefficient than the theoretical ICRU-44 soft-tissue coefficient. Therefore, Lucite attenuated the bone Pb signal more than the porcine tissue, which is also experimentally observed in Figure 1.

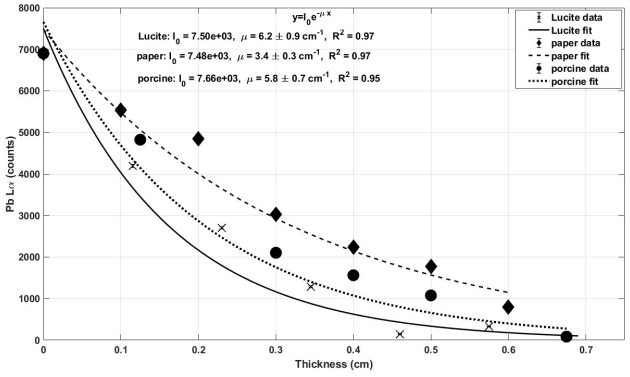

Fig. 1 Pb L_α peak area as a function of soft-tissue thickness (cm) for Lucite, paper, and porcine materials. The uncertainties are smaller than the marker size and are not visible

3.2 Effect of the soft-tissue thickness on the sensitivity and the detection limit

It is important to interpret the effect of soft-tissue thickness on measurement sensitivity within the context of physiologically relevant conditions. At the tibia measurement site, commonly used in *in vivo* bone Pb XRF studies, the overlying soft-tissue thickness typically ranges between (3.6 ± 1.5) mm [26] and (4.8 ± 2.0) mm [27]. In the case of phalanx bone measurements also used in bone

View Article Online
DOI: 10.1039/D6JA00139D

Sr and Pb XRF applications, the average soft-tissue thickness is (2.9 ± 0.7) mm[27]. The range of thicknesses investigated in this work (0–7 mm) was therefore selected to encompass, and slightly exceed, those encountered *in vivo*.

The peak areas of the Pb L_α (10.5 keV) and Pb L_β (12.6 keV) were determined for bare bone HAp phantoms with Pb concentrations ranging from 0 to 100 μg Pb/g Ca. Subsequently, the HAp phantoms were overlaid with Lucite, paper, or porcine tissue to construct calibration phantoms. All calibration curves showed that the Pb peak areas increased proportionally with Pb concentration, exhibiting strong linear relationships, as illustrated in Figure 2.

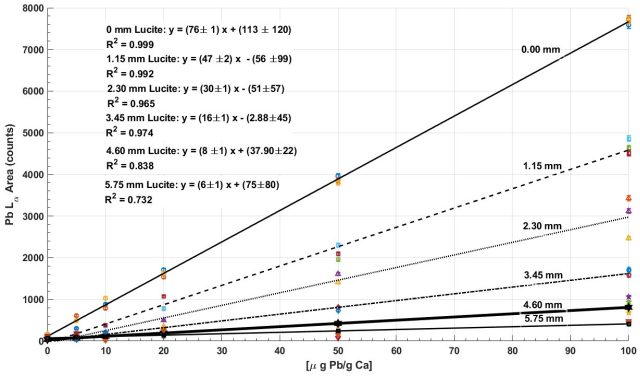

Fig. 2 Example calibration curves obtained by plotting the Pb L_α peak area as a function of Pb concentration using Lucite as the overlying soft-tissue phantom. Calibration curves corresponding to six Lucite thicknesses overlying the HAp bone phantoms are also shown. Each concentration was measured independently in triplicate

To evaluate the sensitivity of the measurements, defined as the slope of the calibration curves (Table 3), it was observed that sensitivity decreased with increasing soft-tissue thickness. Specifically, the sensitivity decreased from 76 counts μg Pb/g Ca for the bare bone phantom to 8 counts μg Pb/g Ca for 4.60 mm of Lucite. Similarly, the sensitivity decreased to 18 and 12 counts μg Pb/g Ca for 5 mm thick paper and porcine tissue, respectively, overlying the HAp phantoms. These results demonstrate a significant reduction in sensitivity with increasing soft-tissue thickness (Figure 2 and Table 3), which represents a key limitation of bone Pb L-XRF measurements using portable XRF systems. This observation is consistent with previous studies[2,7]. Consequently, the reduction in system sensitivity with increasing overlying soft-tissue thickness may limit the applicability of this technique for detecting Pb concentrations near the detection limit.

In addition to sensitivity, the combined MDL from Pb L_α and L_β peaks was calculated in the presence of tissue-mimicking materials and porcine tissue using Equations 1 and 2. As expected, and as shown in Table 3, the MDL increased with increasing soft-tissue thickness. To enable comparison at identical thicknesses, MDL values were extrapolated using fitted functions based on the data in Table 3. The extrapolated results (Table 4) indicate that, for a given thickness, the MDL is highest for Lucite, followed by porcine tissue, and lowest for paper.

Statistical analysis was performed to assess differences in MDL across the tested materials. No statistically significant differences were observed for tissue thicknesses below 5 mm, indicating comparable detection performance among Lucite, paper, and porcine tissue within this range. However, at thicknesses of 5 mm and above, statistically significant differences in MDL were observed, suggesting that additional material-dependent factors influence system performance at greater thicknesses.

It is informative to compare the performance of the present system with earlier L-shell XRF implementations. In 1991, Rosen *et al.*[34] reported a minimum detection limit of approximately 7 μg Pb/g for an overlying soft-tissue thickness of 5 mm using an L-XRF system based on a silver anode X-ray source and a Si(Li) detector, with a measurement time of 16.5 min. In that work, soft-tissue thicknesses in the range of 3–8 mm were explicitly accounted for through attenuation corrections, highlighting the importance of tissue effects in in vivo measurements. In a more recent study by Specht *et al.*[15,35], an XL3t GOLDD+ portable XRF system (Thermo Fisher Scientific Inc., Billerica, MA, USA) was used with a 3 min measurement time, yielding a detection limit comparable to that of our system.

In comparison, the present study demonstrates substantially higher Pb peak areas under similar concentration ranges, despite a significantly shorter acquisition time of 180 s. This improvement can be attributed to advances in detector technology, particularly the use of silicon drift detectors (SDDs), as well as improved excitation and measurement conditions in modern pXRF systems. However, despite these improvements in signal acquisition, attenuation by overlying soft tissue remains a critical factor influencing both sensitivity and detection limits. The results presented here are therefore consistent with earlier findings, while extending them by systematically evaluating the impact of soft-tissue-equivalent materials on Pb quantification accuracy.

Table 3 Sensitivity of Pb L_α [counts/(μg Pb/g Ca)] and experimental minimum detection limits (MDL) [μg Pb/g Ca] for Lucite, paper, and porcine tissue with thicknesses ranging from 1 to 5 mm, representing typical soft-tissue thicknesses at measurement sites (finger and tibia). The uncertainty in thickness is ±0.05 mm

Material	Thickness (mm)	Sensitivity [counts/(μg Pb/g Ca)]	MDL [μg Pb/g Ca]
Lucite			
	0.00	76 ± 1	1.0
	1.15	47 ± 2	1.7
	2.30	30 ± 1	2.4
	3.45	16 ± 1	4.9
	4.60	8 ± 1	9.7
	5.75	6 ± 2	12.5
Paper			
	0.00	76 ± 1	1.0
	1.00	69 ± 1	1.3
	2.00	49 ± 1	1.7
	3.00	37 ± 1	2.2
	4.00	26 ± 1	3.0
	5.00	18 ± 1	4.3
Porcine			
	0.00	76 ± 1	1.0
	1.25	48 ± 1	1.7
	3.00	26 ± 1	2.8
	4.00	17 ± 1	4.4
	5.00	12 ± 1	6.2

View Article Online
DOI: 10.1039/D6JA00139D

Table 4 Extrapolated minimum detection limits (MDL) [μg Pb/g Ca] at integer soft-tissue–equivalent thicknesses (0–5 mm). Values were obtained by piecewise linear interpolation of the measured data and rounded to one decimal place. *p*-values represent comparisons of Lucite and paper MDLs relative to porcine tissue

	MDL (μg Pb/g Ca)		
Thickness (mm)	**Lucite**	**Paper**	**Porcine**
0.00	1.0	1.0	1.0
1.00	1.6	1.3	1.5
2.00	2.2	1.7	2.2
3.00	3.9	2.2	2.8
4.00	7.2	3.0	4.4
5.00	10.6	4.3	6.2
p-value vs porcine	0.4610	0.4351	–

3.3 Bone lead quantification of cadaver tibiae

The spectra and the regions surrounding the Pb signals for tibia #1 with different soft-tissue mimicking materials are shown in Figure 3. The spectra demonstrate that the Pb L$_\alpha$ (10.5 keV) and Pb L$_\beta$ (12.6 keV) peaks are well separated from the Compton peak (∼20.8 keV), thereby reducing background interference and highlighting the advantage of using a silver-anode pXRF system for bone Pb measurements.

In addition to Pb, other elements present in the tibia, including Ca, Fe, Ni, and Zn, are also identified in Figure 3.

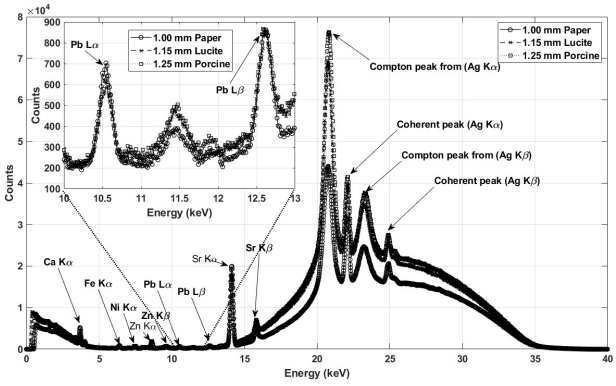

Fig. 3 Spectra of cadaver tibia #1 covered with Lucite, paper and porcine tissues of similar thickness and zoom-in between 10 and 13 keV to show Pb L$_\alpha$ (10.5 keV) and Pb L$_\beta$ (12.6 keV)

The MDL values of the bone Pb pXRF measurements suggest that Lucite or paper, as the soft-tissue material, can be added to the bone phantoms to create phantoms for direct calibration. If bone-soft-tissue phantoms are created, human *in vivo* bone Pb quantification can be achieved once the overlying soft-tissue thickness at the subject's tibia is known, by using the direct calibration curve generated with the equivalent soft-tissue materials thickness overlying the HAp bone phantom. This approach, however, would require multiple calibration curves since human tissue thicknesses can have many values, which is not practical. Therefore, other approaches to quantifying Pb in human bone were proposed in the literatures.

In our study, three quantification approaches—direct quantification, the adjusted coherent normalization, and the Compton interpolation—were applied. Example calculations for determining Pb concentrations in postmortem human tibia #1 are presented to illustrate each method. The calibration equations of Pb L$_\beta$ are listed in Table 5, while the Pb L$_\beta$, Compton and coherent peak areas are given in Table 6.

Direct quantification: The direct calibration requires generating multiple calibration equations with many soft-tissue mimicking material thicknesses covering the HAp bone Pb phantoms. In this work, calibration curves were generated for each material of known thickness using the bone HAp phantoms. Examples of the calibration equations for two thicknesses are summarized in Table 5 using the Pb L_β peak. The calibration equations were then used to determine the Pb concentration in the human tibiae based on their measured Pb peak area and the known overlying soft-tissue material thickness. For Tibia #1, for example, the Pb quantification based on the Pb L_β peak was performed as follows:

The Pb L$_\beta$ calibration equation for 1.25 mm paper is given by $y = (50.8 \pm 1.4)x + (89.8 \pm 21.6)$, where y is the Pb peak area (counts) and x is the Pb concentration (μg Pb/g Ca).

From Table 6, the measured peak area of Tibia #1 covered with 1.25 mm porcine tissue was $y = (3.07 \times 10^3 \pm 3.80 \times 10^2)$ counts, which corresponds to a bone Pb concentration of $x = (58.7 \pm 7.7)$ μg Pb/g Ca.

Using the direct quantification method based on Pb L_α and Pb L_β, the Pb concentrations for the three cadaveric tibiae are shown in Table 7, where the shown bone Pb concentration is the inverse weighted average of the L_α and L_β based estimates.

Table 5 Regression parameters for Pb L$_\beta$ peak area [counts] as a function of Pb concentration [μg Pb/g Ca] for 1.25, 3.00, and 5.00 mm of Lucite and paper overlying HAp bone phantoms. Uncertainties represent standard errors.

Sample	**Slope [counts/(μg Pb/g Ca)]**	**Intercept (counts)**	R^2
Bare HAp	76.0 ± 1.4	113 ± 120	0.999
Paper 1.25 mm	50.8 ± 1.4	89.8 ± 21.6	0.998
Paper 3.00 mm	32.0 ± 4.0	110 ± 310	0.977
Paper 5.00 mm	22.0 ± 4.0	-270 ± 90	0.977
Lucite 1.25 mm	46.0 ± 4.0	0 ± 200	0.989
Lucite 3.00 mm	33.0 ± 9.0	200 ± 400	0.822
Lucite 5.00 mm	24.0 ± 4.0	180 ± 250	0.998

Table 6 Characteristic Pb L_β, Compton and coherent peak area, and their propagated uncertainties for Tibia #1 measured with 1.25 mm porcine assumed to closely resemble an *in vivo* bone Pb measurements

Quantity	**Counts**
L_β peak area	3.07×10^3
L_β uncertainty	3.80×10^2
Compton peak area	2.51×10^6
Compton uncertainty	2.21×10^4
Coherent peak area	3.79×10^5
Coherent uncertainty	1.38×10^4

Adjusted coherent normalization: The adjusted coherent normalization method, adopted from Gevaert and Chettle[28], was used as the second quantification approach to determine Pb concentration in the cadaver tibiae. The equivalent Lucite and paper thicknesses corresponding to the porcine tissue thickness were

View Article Online
DOI: 10.1039/D6JA00139D

determined from the variation of the Compton peak area as a function of material thickness (Figure 4). The dependence of the coherent peak area on Lucite and paper thickness for the 100 μg Pb/g Ca HAp bone phantom (Figure 5) was then used to estimate the unattenuated coherent peak area. In addition, the ratio of the Pb L_β peak area to the coherent peak area as a function of Pb concentration in the HAp phantom (Figure 6) was used to establish the calibration relationship.

Using the procedure described in Section 2.4, the Pb concentration in Tibia #1 was determined as follows:

1. Using the Compton peak area as a function of paper and Lucite thickness (Figure 4 and Table 6), the 1.25 mm porcine tissue with a Compton peak area of $(2.51 \times 10^6 \pm 2.21 \times 10^4)$ is equivalent to (1.65 ± 0.08) mm of Lucite and (5.69 ± 1.08) mm of paper.

2. The Pb L_β and Compton peak areas for Tibia #1 covered with 1.25 mm porcine tissue are listed in Table 6.

3. The Pb L_β peak area for 100 μg Pb/g Ca as a function of Lucite and paper thickness (Figure 7) is given by:

$$L_{\beta,\text{Lucite}} = (7.68 \times 10^3 \pm 4.1 \times 10^1)\, e^{-(0.406 \pm 0.003)x}$$
$$L_{\beta,\text{paper}} = (7.16 \times 10^3 \pm 4.5 \times 10^1)\, e^{-(0.208 \pm 0.006)x}$$

Similarly, the variation of the coherent peak area with material thickness (Figure 5) is expressed as:

$$I_{\text{coh,Lucite}} = (3.77 \times 10^5)\, e^{0.0821x}$$
$$I_{\text{coh,paper}} = (3.27 \times 10^5)\, e^{-0.0109x}$$

Using the equivalent thicknesses of Lucite and paper determined in step 1, the Pb L_β and coherent peak areas corrected to the bare bone (using the Beer–Lambert attenuation law) are:

$$L_{\beta,\text{Lucite, bare}} = (4.88 \pm 0.62) \times 10^3 \text{ counts}$$
$$L_{\beta,\text{paper, bare}} = (1.00 \pm 0.25) \times 10^4 \text{ counts}$$
$$I_{\text{coh,Lucite, bare}} = (3.47 \pm 0.13) \times 10^5 \text{ counts}$$
$$I_{\text{coh,paper, bare}} = (3.57 \pm 0.08) \times 10^5 \text{ counts}$$

4. From Figure 6, the Pb L_β-to-coherent peak ratio as a function of Pb concentration was used to establish the calibration equation for bare HAp:

$$\frac{L_\beta}{\text{Coherent}} = (2.17 \pm 0.06) \times 10^{-4} C + (8.60 \pm 1.10) \times 10^{-4}$$

where C is the Pb concentration in $\mu g/g$.

Using this calibration, the estimated bone Pb concentrations for Tibia #1 were (75.1 ± 12.6) μg/g and (156.0 ± 44.0) μg/g for Lucite and paper, respectively. Results obtained using the adjusted coherent normalization method for all tibiae are summarized in Table 7. For each measurement condition, the reported Pb concentration corresponds to the inverse-variance weighted average of the independent estimates derived from the Pb L_α and Pb L_β peaks.

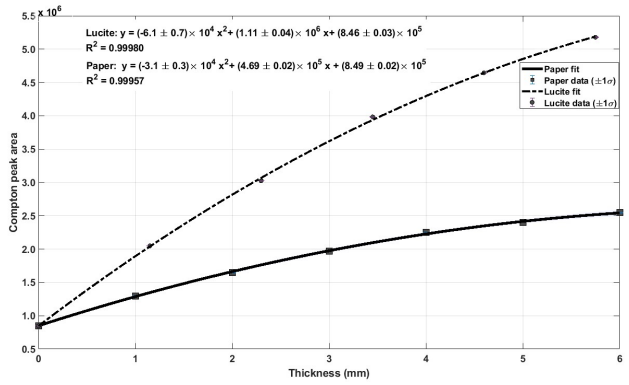

Fig. 4 Compton peak area of the 100 μg Pb/g Ca bone phantom as a function of Lucite and paper thickness. The uncertainty of each data point is smaller than the marker size and is therefore not visible

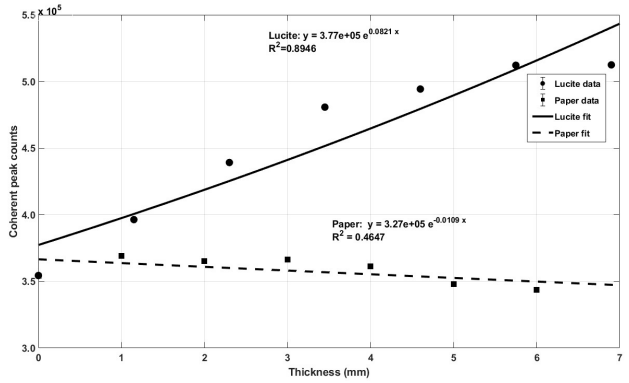

Fig. 5 Coherent peak area of the 100 μg Pb/g Ca bone phantom as a function of Lucite and paper thickness. The uncertainty of each data point is smaller than the marker size and is therefore not visible

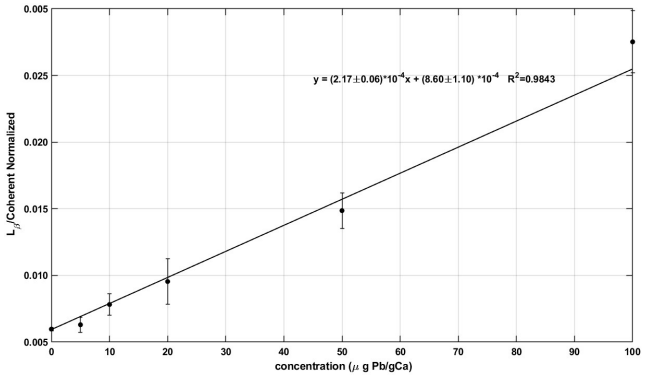

Fig. 6 Ratio of Pb L_β to coherent peak area as a function of Pb concentration (μg Pb/g Ca) for bare bone phantoms. The solid line represents the calibration curve for the HAp bone phantom

Compton interpolation: The Compton interpolation method used to determine the Pb concentration was adapted from the work of Specht et al.[7,15,29]. Using the tibia #1 data (Table 6) and

View Article Online
DOI: 10.1039/D6JA00139D

following the procedure outlined in Section 2.4, the Pb concentration in tibia #1 was determined as:

1. Using the Compton peak area measured for Tibia #1, a porcine soft-tissue thickness of 1.25 mm was determined to be equivalent to (1.65 ± 0.08) mm of Lucite and (5.69 ± 1.08) mm of paper, as obtained in Step i of the adjusted coherent normalization method.

2. Based on the fitted relationships describing the variation of the Pb L_β peak area as a function of Lucite and paper thickness (Figure 7), the Pb L_β peak areas corresponding to these equivalent Lucite and paper thicknesses were extrapolated to be (4268 ± 98) counts and (1955 ± 488) counts, respectively.

3. Using Equation 3, the resulting Pb concentration for Tibia #1 was calculated to be (71.9 ± 9.1) μg Pb/g Ca when Lucite was used as the soft-tissue material and (157.0 ± 43.8) μg Pb/g Ca when paper was used.

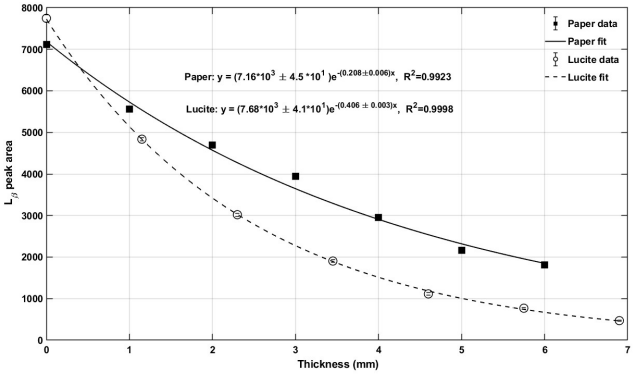

Fig. 7 Pb L_β peak area as function of Lucite and paper thicknesses covering 100 μg Pb/g Ca bone phantom. The uncertainty of each data point is smaller than the marker size and is therefore not visible

The results of bone Pb quantification for three human tibiae are summarized in Table 7. The reported concentrations correspond to the weighted average of the independent Pb estimates derived from the Pb L_α and Pb L_β peaks. The table includes the Pb concentrations determined with the three quantification approaches and their associated *p*-values when compared to the bare tibia Pb. For all three tibiae, the bone concentrations determined with different thicknesses of Lucite were statistically identical to the corresponding bare tibia Pb concentration for each quantification approach ($p > 0.05$), indicating that Lucite is a suitable soft-tissue phantoms. In contrast, when paper was used as the soft-tissue material, the calculated Pb concentrations were consistently and significantly different from the corresponding bare tibia values at all tested thicknesses and for all three quantification methods ($p < 0.05$). Paper-based measurements were not available for the 5 mm porcine, as the required paper thickness exceeded the practical thickness limit (greater than 6 mm), rendering reliable extrapolation of Pb concentration infeasible.

Furthermore, comparison of the direct, adjusted coherent normalization, and Compton interpolation methods across different tissue materials thicknesses for the higher-Pb tibiae (Tibia #1 and Tibia #2) using Lucite showed that the percent difference between the extrapolated Pb concentrations and the corresponding bare tibia values decreased with decreasing porcine thickness. This trend is attributed to reduced attenuation of the Pb signal at lower thicknesses, and thus no statistically significant differences were observed ($p > 0.05$). In contrast, for Tibia #3, which exhibited lower Pb concentrations, all three quantification methods yielded Pb values that were statistically different from the bare Tibia #3 Pb concentration. This finding indicates a limitation in the ability of these methods to accurately extrapolate Pb concentrations under the low Pb signal conditions, particularly when the bone Pb concentration approaches the minimum detection limit (MDL).

In contrast, analysis of Tibia #1 and Tibia #2 covered with varying Lucite thicknesses showed that all three quantification methods were able to estimate the tibial Pb concentrations with differences of less than 25% relative to the corresponding bare measurements. The largest percent differences were observed for Tibia #3, particularly when covered with a 5 mm porcine-equivalent thickness. These results indicate that the ability to quantify tibial Pb depends on both the overlying soft-tissue thickness and the present Pb concentration.

The results of this study indicate that, beyond elemental composition, material density is a key factor in determining the suitability of soft-tissue substitutes for *in vivo* bone Pb L-shell XRF measurements. Although the mass attenuation coefficient (μ/ρ) characterizes photon interactions on a per-mass basis, the experimentally relevant quantity is the linear attenuation coefficient, $\mu = \rho(\mu/\rho)$, which depends directly on material density. The substantially lower density of paper (0.82 g/cm^3) compared to Lucite (1.18 g/cm^3) and porcine tissue (1.19 g/cm^3) results in reduced attenuation and scattering for a given material thickness. In contrast, the similar densities of Lucite and porcine tissue produce more comparable photon interaction conditions. These findings suggest that the improved performance of Lucite arises predominately from its similarity in bulk density to biological soft tissue, in addition to its compositional characteristics.

The large discrepancies observed between quantification approaches when using paper as a soft-tissue substitute can likely be attributed to the combined effects of density mismatch and altered scattering conditions. Both the adjusted coherent normalization and Compton interpolation approaches assume a consistent relationship between scatter signal intensity and overlying mass thickness. These methods utilize the variation in Compton peak area with material thickness to estimate equivalent soft-tissue thickness, following the approach proposed by Nie *et al.*[3]. However, due to the lower density of paper and the resulting differences in photon scattering behaviour, this assumption is not maintained, leading to a systematic overestimation of the effective tissue thickness relative to Lucite and porcine tissue.

Furthermore, the results obtained for Tibia #3, which exhibited the lowest Pb concentration, indicate that the technique becomes increasingly sensitive to systematic errors at low Pb signal

View Article Online
DOI: 10.1039/D6JA00139D

Table 7 Comparison of tibial Pb concentrations (μg Pb/g Ca) obtained using the direct, Compton interpolation, and coherent normalization methods at different soft-tissue thicknesses. Values represent the inverse weighted average of Pb L_α and Pb L_β. Percent differences were calculated relative to the bare tibia Pb concentration. Asterisks (*) indicate statistically significant differences ($p < 0.05$).

Tibia	Soft tissue	Method	Calculated tibia [Pb]	Calculated SD	Bare tibia [Pb]	Bare SD	% Diff vs bare	p-value
1.25 mm porcine								
#1	Paper	Direct	65.1	6.9	83.6	6.0	−22.1	0.025*
#1	Paper	Coherent norm.	173.0	39.9	83.6	6.0	+106.9	0.018*
#1	Paper	Compton interp.	186.2	34.2	83.6	6.0	+122.8	0.007*
#1	Lucite	Direct	74.2	8.9	83.6	6.0	−11.2	0.204
#1	Lucite	Coherent norm.	89.7	10.5	83.6	6.0	+7.3	0.432
#1	Lucite	Compton interp.	79.7	7.7	83.6	6.0	−4.7	0.527
#2	Paper	Direct	55.8	2.3	65.2	5.3	−14.4	0.048*
#2	Paper	Coherent norm.	127.9	24.1	65.2	5.3	+96.2	0.012*
#2	Paper	Compton interp.	145.4	24.7	65.2	5.3	+123.1	0.005*
#2	Lucite	Direct	65.8	7.3	65.2	5.3	+0.9	0.914
#2	Lucite	Coherent norm.	64.5	7.0	65.2	5.3	−1.1	0.897
#2	Lucite	Compton interp.	68.0	7.5	65.2	5.3	+4.3	0.625
#3	Paper	Direct	10.5	1.1	14.9	1.4	−29.5	0.013*
#3	Paper	Coherent norm.	30.0	2.5	14.9	1.4	+101.3	0.001*
#3	Paper	Compton interp.	33.5	3.0	14.9	1.4	+124.8	0.001*
#3	Lucite	Direct	11.6	1.2	14.9	1.4	−22.1	0.036*
#3	Lucite	Coherent norm.	30.0	7.5	14.9	1.4	+101.3	0.027*
#3	Lucite	Compton interp.	33.5	8.0	14.9	1.4	+124.8	0.017*
3.00 mm porcine								
#1	Paper	Direct	62.7	6.2	83.6	6.0	−25.0	0.014*
#1	Paper	Coherent norm.	127.6	22.8	83.6	6.0	+52.6	0.032*
#1	Paper	Compton interp.	152.8	30.5	83.6	6.0	+82.8	0.018*
#1	Lucite	Direct	63.6	22.2	83.6	6.0	−23.9	0.206
#1	Lucite	Coherent norm.	76.5	10.1	83.6	6.0	−8.5	0.354
#1	Lucite	Compton interp.	70.6	9.7	83.6	6.0	−15.6	0.120
#2	Paper	Direct	51.6	2.2	65.2	5.3	−20.9	0.015*
#2	Paper	Coherent norm.	123.5	34.2	65.2	5.3	+89.4	0.043*
#2	Paper	Compton interp.	140.5	46.2	65.2	5.3	+115.6	0.049*
#2	Lucite	Direct	58.0	7.8	65.2	5.3	−11.0	0.257
#2	Lucite	Coherent norm.	56.0	18.1	65.2	5.3	−14.1	0.446
#2	Lucite	Compton interp.	64.9	19.1	65.2	5.3	−0.5	0.980
#3	Paper	Direct	11.9	1.2	14.9	1.4	−20.1	0.048*
#3	Paper	Coherent norm.	36.6	12.5	14.9	1.4	+145.6	0.040*
#3	Paper	Compton interp.	55.2	23.1	14.9	1.4	+270.5	0.039*
#3	Lucite	Direct	11.5	1.3	14.9	1.4	−22.8	0.037*
#3	Lucite	Coherent norm.	19.5	2.4	14.9	1.4	+30.9	0.046*
#3	Lucite	Compton interp.	25.5	3.4	14.9	1.4	+71.1	0.008*
5.00 mm porcine								
#1	Lucite	Direct	87.8	41.7	83.6	6.0	+5.0	0.184
#1	Lucite	Coherent norm.	88.7	62.7	83.6	6.0	+6.1	0.175
#1	Lucite	Compton interp.	85.9	61.5	83.6	6.0	+2.8	0.175
#2	Lucite	Direct	70.2	16.2	65.2	5.3	+7.7	0.330
#2	Lucite	Coherent norm.	62.6	25.1	65.2	5.3	−4.0	0.252
#2	Lucite	Compton interp.	60.4	24.4	65.2	5.3	−7.4	0.256
#3	Lucite	Direct	37.7	2.5	14.9	1.4	+153.0	< 0.001*
#3	Lucite	Coherent norm.	23.0	2.7	14.9	1.4	+54.4	0.009*
#3	Lucite	Compton interp.	29.3	3.6	14.9	1.4	+96.6	0.002*

levels. The statistically significant differences observed across all quantification methods and tissue thicknesses suggest that small inaccuracies in attenuation correction, scatter normalization, and counting statistics have a proportionally larger impact near the detection limit. This finding highlights an important limitation of the Pb L-shell pXRF method, namely reduced reliability for quantifying low bone Pb concentrations, which is particularly relevant for *in vivo* applications involving populations with low lead exposure.

Overall, the results indicate that, under the tested experimental conditions, Lucite provides a more appropriate soft-tissue surrogate than paper. In addition, any of the three quantification methods can be used to estimate tibial Pb concentrations, provided that the limitations imposed by the limit of quantification are taken into account. These results are consistent with those reported by Specht et al., who used Lucite as a soft-tissue surrogate for calibrating pXRF systems in *in vivo* studies[7,15]. In contrast, although paper has been suggested as a suitable soft-tissue surrogate for Sr measurements[28], our findings demonstrate that the use of paper results in statistically significant differences between the measured tibial Pb concentrations and the corresponding extrapolated values.

Although all measurements were performed using the same detection system, cadaver bones, and phantoms, and efforts were made to maintain consistent positioning and contact geometry, geometric effects may still have contributed to the observed differences and represent an inherent limitation of experimental pXRF measurements. Finally, although this study used a new and more powerful portable XRF spectrometer, the observed attenuation and scattering effects are not specific to portability of the XRF device. They arise from Pb L-shell X-ray energies, soft-tissue attenuation, detector sensitivity, and measurement geometry, and are, therefore, applicable to XRF-based bone Pb quantification based on the L-shell X-rays more broadly.

4 Conclusions

This study investigated the suitability of Lucite and paper as soft-tissue mimicking materials for the *in vivo* quantification of bone Pb using portable X-ray fluorescence (pXRF) spectrometry. Comparison of Lucite and paper against porcine tissue, which closely

View Article Online
DOI: 10.1039/D6JA00139D

approximates the attenuation characteristics of human soft tissue, demonstrated that Lucite more effectively reproduces the attenuation behavior of soft tissue within the Pb L-shell energy range. The results further demonstrates that the thickness of the overlying soft tissue significantly influences the detection limit of the pXRF system, with increasing thickness leading to higher MDL and lower sensitivity. Additionally, the adjusted coherent normalization and Compton interpolation methods were shown to provide effective Pb quantification in cadaver tibiae covered with porcine tissue, provided that limitations associated with low Pb concentrations are appropriately considered. The statistical comparisons should be interpreted with caution due to the limited sample size ($n = 3$), which reduces the power of Welch's t-test to detect small differences. Accordingly, the results support observed trends rather than definitive conclusions.

Acknowledgements

The Natural Science and Engineering Research Council of Canada (NSERC) is acknowledged for their financial support through a Discovery Grant (EDS). The Faculty of Science at Toronto Metropolitan University is also acknowledged for their financial support of this work (EDS).

References

1 A. J. Specht, D. W. Steadman, M. Davis, S. M. Bartell and M. G. Weisskopf, *The Science of the Total Environment*, 2023, **880**, 163197–163197.

2 E. Da Silva, G. Mankovskii, B. Kirkham, J. Groves, M. Gherase, D. E. B. Fleming and A. Pejović-Milić, *Advances in X-ray Analysis*, 2018, **61**, 116–121.

3 L. H. Nie, S. Sanchez, K. Newton, L. Grodzins, R. O. Cleveland and M. G. Weisskopf, *Physics in Medicine and Biology*, 2011, **56**, N39–N51.

4 X. Zhang, E. M. Wells, A. J. Specht, M. G. Weisskopf, J. Weuve and L. H. Nie, *Journal of Trace Elements in Medicine and Biology*, 2022, **74**, 127077.

5 A. T. Al-Kazwini and N. A. Al-Masoudi, *Journal of Physics: Conference Series*, 2020, **1644**, 012029.

6 R. A. M. P. Gomes, A. L. Santos and L. Catarino, *International Journal of Paleopathology*, 2024, **44**, 85–89.

7 A. J. Specht, C. Hoover and T. Grier, *Current Environmental Health Reports*, 2024, **11**, 443–451.

8 Centers for Disease Control and Prevention (CDC), *Lead*, `https://www.cdc.gov/nceh/lead/default.htm`, 2022.

9 B. P. Lanphear, R. Hornung, J. Khoury, K. Yolton, P. Baghurst, D. C. Bellinger, R. L. Canfield, K. N. Dietrich, R. Bornschein, T. Greene, S. J. Rothenberg, H. L. Needleman, L. Schnaas, G. Wasserman, J. Graziano and R. Roberts, *Environmental Health Perspectives*, 2005, **113**, 894–899.

10 L. Wang, C. Wang, T. Liu, H. Xuan, X. Li, X. Shi, F. Dai, J. Chen, D. Li and T. Xu, *Archives of Public Health = Archives Belges de Santé Publique*, 2023, **81**, 146.

11 B. P. Lanphear, S. Rauch, P. Auinger, R. W. Allen and R. W. Hornung, *The Lancet Public Health*, 2018, **3**, e177–e184.

12 International Commission on Radiological Protection, *ICRP Publication 134: Occupational Intakes of Radionuclides: Part 2*, SAGE Publications, Newbury Park, CA, 2016.

13 F. E. McNeill, M. Fisher, D. R. Chettle, M. Inskip, N. Healey, R. Bray, C. E. Webber, W. I. Manton, L. Marro and T. E. Arbuckle, *Physiological Measurement*, 2018, **39**, 015005.

14 H. Nie, D. R. Chettle, E. M. F and J. M. O'Meara, *Physics in Medicine and Biology*, 2004, **49**, N325–N334.

15 A. J. Specht, M. Weisskopf and L. H. Nie, *Journal of Biomarkers*, 2014, **2014**, 1–9.

16 A. J. Specht, F. Mostafaei, Y. Lin, J. Xu and L. H. Nie, *Applied Spectroscopy*, 2017, **71**, 1962–1968.

17 E. Da Silva, B. Kirkham, D. V. Heyd and A. Pejović-Milić, *Analytical Chemistry*, 2013, **85**, 9189–9195.

18 L. M. Bickley, E. Da Silva, D. R. Chettle and F. E. McNeill, *Journal of Analytical Atomic Spectrometry*, 2025, **40**, 1086–1097.

19 ICRU, *Report 44 of the International Commission on Radiation Units and Measurements*, 1989, **–**, —.

20 C. M. Heirwegh, D. R. Chettle and A. Pejović-Milić, *Physics in Medicine & Biology*, 2010, **55**, 1083–1098.

21 H. Moise, D. R. Chettle and A. Pejović-Milić, 2014, **61**, 48–54.

22 R. C. N. Studinski, F. E. McNeill, D. R. Chettle and J. M. O'Meara, *Phys. Med. Biol.*, 2005, **50**, 521–530.

23 D. E. B. Fleming, M. R. Gherase and K. M. Alexander, *X-ray Spectrometry*, 2011, **40**, 343–347.

24 E. Da Silva, D. V. Heyd, B. Rizvi and A. Pejović-Milić, *Biomedical Physics & Engineering Express*, 2016, **2**, 015006.

25 M. Micsa, D. Ha and E. Da Silva, *Biomedical Physics & Engineering Express*, 2024, **10**, 15001.

26 A. J. Specht, A. S. Dickerson and M. G. Weisskopf, *Environmental Research*, 2019, **172**, 273–278.

27 A. Pejović-Milić, J. A. Brito, J. B. Gyorffy and D. R. Chettle, *Medical Physics*, 2002, **29**, 2687–2691.

28 J. Gevaert and D. R. Chettle, *X-Ray Spectrometry*, 2019, **48**, 443–451.

29 X. Zhang, A. J. Specht, E. Wells, M. G. Weisskopf, J. Weuve and L. H. Nie, *The Science of the Total Environment*, 2021, **753**, 142351.

30 L. J. Somervaille, D. R. Chettle and M. C. Scott, *Physics in Medicine and Biology*, 1985, **30**, 929–943.

31 E. Da Silva, A. Pejović-Milić and D. V. Heyd, *Journal of Analytical Atomic Spectrometry*, 2008, **23**, 527–534.

32 National Institute of Standards and Technology, *X-Ray Mass Attenuation Coefficients*, `https://physics.nist.gov/PhysRefData/XrayMassCoef/tab2.html`, Accessed February 8, 2026.

33 National Institute of Standards and Technology, *X-Ray Mass Attenuation Coefficients*, `https://physics.nist.gov/PhysRefData/XrayMassCoef/tab3.html`, Accessed February 8, 2026.

34 J. F. Rosen, M. E. Markowitz, P. E. Bijur, S. T. Jenks, L. Wielopolski, J. A. Kalef-Ezra and D. N. Slatkin, *Environmental Health Perspectives*, 1991, **91**, 57–62.

35 A. J. Specht, O. O. Ogunseitan, K. L. Weisskopf and M. G.

View Article Online
DOI: 10.1039/D6JA00139D

Weisskopf, *Physiological Measurement*, 2018, **39**, 085007.

View Article Online
DOI: 10.1039/D6JA00139D

The raw data is available using the following link.

https://drive.google.com/drive/folders/1zbs6NFlEOe5GChXXkrQDXZsRJIz6WNsA?usp=sharing